OXFORD

Human Molecular Genetics, 2017, Vol. 26, No. 12 2231–2246

doi: 10.1093/hmg/ddx114
Advance Access Publication Date: 24 March 2017
Original Article

ORIGINAL ARTICLE

Sodium butyrate rescues dopaminergic cells from alpha-synuclein-induced transcriptional deregulation and DNA damage

Isabel Paiva[1,†], Raquel Pinho[1,2,†], Maria Angeliki Pavlou , Magali Hennion[3], Pauline Wales[1], Anna-Lena Schütz[3], Ashish Rajput[3], Éva M. Szegő[1], Cemil Kerimoglu[4], Ellen Gerhardt[1], Ana Cristina Rego[5,6], André Fischer[4,7], Stefan Bonn[3] and Tiago F. Outeiro[1,8,9,*]

[1]Department of Experimental Neurodegeneration, Center for Nanoscale Microscopy and Molecular Physiology of the Brain, Center for Biostructural Imaging of Neurodegeneration, University Medical Center Göttingen, 37073, Göttingen, Germany, [2]Faculty of Medicine, University of Porto, 4099-002 Porto, Portugal, [3]Department of Computational Systems Biology, German Center for Neurodegenerative Diseases (DZNE), 37077 Göttingen, Germany, [4]Department of Epigenetics and Systems Medicine in Neurodegenerative Diseases, German Center for Neurodegenerative Diseases (DZNE), 37077 Göttingen, Germany, [5]Department of Neuroscience and Disease, Center for Neuroscience and Cell Biology, University of Coimbra, 3004-504, Coimbra, Portugal, [6]Faculty of Medicine, University of Coimbra, 3000-354 Coimbra, Portugal, [7]Department of Psychiatry and Psychotherapy, University Medical Center Göttingen, 37077 Göttingen, Germany, [8]CEDOC – Chronic Diseases Research Center, Faculdade de Ciências Médicas, Universidade Nova de Lisboa, Lisboa, Portugal and [9]Max Planck Institute for Experimental Medicine, 37075 Göttingen, Germany

*To whom correspondence should be addressed at: Department of Experimental Neurodegeneration, University Medical Center Göttingen, Waldweg 33, 37073, Göttingen, Germany. Tel: +49 5513913544; Fax: +49 5513922693; Email: touteir@gwdg.de

Abstract

Alpha-synuclein (aSyn) is considered a major culprit in Parkinson's disease (PD) pathophysiology. However, the precise molecular function of the protein remains elusive. Recent evidence suggests that aSyn may play a role on transcription regulation, possibly by modulating the acetylation status of histones. Our study aimed at evaluating the impact of wild-type (WT) and mutant A30P aSyn on gene expression, in a dopaminergic neuronal cell model, and decipher potential mechanisms underlying aSyn-mediated transcriptional deregulation. We performed gene expression analysis using RNA-sequencing in Lund Human Mesencephalic (LUHMES) cells expressing endogenous (control) or increased levels of WT or A30P aSyn. Compared to control cells, cells expressing both aSyn variants exhibited robust changes in the expression of several genes, including downregulation of major genes involved in DNA repair. WT aSyn, unlike A30P aSyn, promoted DNA damage and increased levels of phosphorylated p53. In dopaminergic neuronal cells, increased aSyn expression led to reduced levels of acetylated histone 3. Importantly, treatment with sodium butyrate, a histone deacetylase inhibitor (HDACi), rescued WT

[†]The authors wish it to be known that, in their opinion, the first two authors should be regarded as joint First Authors.
The data set generated in this study has been submitted to the GEO database (GEO Series accession number GSE89115).
Received: November 26, 2016. **Revised:** January 28, 2017. **Accepted:** March 19, 2017

aSyn-induced DNA damage, possibly via upregulation of genes involved in DNA repair. Overall, our findings provide novel and compelling insight into the mechanisms associated with aSyn neurotoxicity in dopaminergic cells, which could be ameliorated with an HDACi. Future studies will be crucial to further validate these findings and to define novel possible targets for intervention in PD.

Introduction

Parkinson's disease (PD) is a complex neurodegenerative condition, associated with a broad range of motor (1) and non-motor symptoms (2). The precise molecular mechanisms leading to PD are still elusive, but mounting evidence suggests a crucial role for alpha-synuclein (aSyn), the main protein component of Lewy bodies, a pathological hallmark of the disorder (3). In addition, point mutations as well as multiplications in the gene encoding for aSyn are associated with familial forms of PD.

Since the association of aSyn with PD, the protein has been widely investigated, and has been linked to a multitude of cellular pathways, such as synaptic transmission, mitochondria homeostasis, and protein degradation, but there is still no consensus regarding its precise function. Recent reports suggest a possible role of aSyn on transcription regulation (4,5), a vital cellular mechanism found deregulated in PD patients (6,7) and in mouse models of the disease (8). However, the genes and pathways regulated by aSyn are also unclear. While some studies postulate that aSyn regulates gene expression in order to confer cellular protection (9,10), others report a deregulation of key pro-survival genes (11,12). Additionally, although deregulation of some genes is attributed to both wild-type (WT) and mutant aSyn (13,14), expression changes in other genes occur only in the presence of the WT or A30P aSyn (15). Thus, our primary goal was to assess the effect of increased levels of WT and A30P mutant aSyn on gene expression in dopaminergic cells.

Since aSyn was previously shown to modulate histone acetylation levels, we investigated whether this related to gene expression changes induced by aSyn. As we have recently reviewed (16), aSyn co-localizes with and binds to histones, in mice (17). In response to stress, increased levels of acetylated histone 3 (acH3) are observed in yeast expressing aSyn (18). In contrast, in SH-SY5Y cells and in transgenic flies, both WT and mutant aSyn promote histone 3 hypoacetylation and toxicity, which is reduced upon treatment with histone deacetylase inhibitors (HDACi) (19). HDAC inhibition is used as an efficient therapeutic strategy against cancer. In these cells, HDACi modulate gene expression, promote DNA damage and DNA repair impairment, and increase oxidative stress (20,21). Conversely, in neurons, HDACi confer protection against oxidative stress (20,21) and protect neurons in a mouse model of PD (22). Conflicting effects were found in dopaminergic neurons (23), thereby arguing for the great need for additional studies.

Our study explored the impact of WT and A30P aSyn on gene expression, in dopaminergic cells. We aimed at deciphering the mechanisms associated with aSyn-induced transcriptional deregulation and whether HDACi could be used to prevent neuronal toxicity associated with increased expression of aSyn.

We demonstrate that in Lund Human Mesencephalic (LUHMES) cells, a dopaminergic neuronal cell line (24), WT and A30P aSyn promoted extensive transcription deregulation. Interestingly, cells expressing aSyn exhibited a significant downregulation of key genes involved in DNA repair. We found that increased expression of WT aSyn induces DNA damage, which is not observed upon expression of A30P aSyn, possibly due to distinct biochemical properties of the protein. We also found that histone 3 hypoacetylation may be involved in aSyn-induced DNA damage. Treatment of dopaminergic neurons with the HDACi sodium butyrate (NaB) rescued WT aSyn expressing cells from DNA damage, possibly by restoring the expression of DNA-repair genes.

Our findings provide new insight into a putative role of aSyn in transcription deregulation, and suggest that treatment with HDACi may regulate gene expression changes related to DNA damage response. Additional studies will be crucial to further validate these findings and to define novel possible targets for intervention in PD.

Results

aSyn induces transcriptional deregulation in dopaminergic neurons

Eight days after differentiation naïve LUHMES cells were immunostained in order to verify the expression of neuronal dopaminergic markers. Microtubule-associated protein 2 (MAP2) and neuron-specific class III β-tubulin (TUJ1) staining revealed an extensive axonal/dendritic network, largely positive for tyrosine hydroxylase (TH). At this stage of differentiation, we also observed endogenous expression of aSyn (Fig. 1A). To investigate the impact of WT and A30P aSyn on gene expression, LUHMES cells were infected using equimolar concentrations of lentivirus encoding for WT aSyn-IRES-GFP, A30P aSyn-IRES-GFP or GFP, as a control (Fig. 1B). Each cell line was treated as described in Figure 1B. We then used fluorescence activated cell sorting to select the green fluorescent cells, resulting in highly homogeneous green-positive, TH-positive neuronal populations (Fig. 1C). The level of aSyn immunosignal was stronger in WT and A30P aSyn cells, and was distributed throughout the cell, including the soma and neurites (Fig. 1D). Using immunoblot analyses, we unequivocally confirmed that expression of aSyn was significantly higher in both WT and A30P aSyn, compared to control cells (Fig. 1F and G).

RNA was extracted from differentiated LUHMES cells stably expressing GFP, WT aSyn, or A30P aSyn, and processed in parallel to avoid bias induced by sample handling. The quality of the RNA was assessed using a Bioanalyzer before proceeding with library preparation and RNA-sequencing (RNA-seq). Extensive quality control of the sequencing data was performed prior to differential analysis.

We identified differential gene expression between control cells and those expressing WT or A30P aSyn (Supplementary Material, Tables S1 and S2). As expected, the gene encoding for aSyn, *SNCA*, exhibited the highest significance and fold-change (FC) increase in both comparisons [$\log_2$FC = 4.06, *p-adjusted* value (*padj*)=2.27E-228 for control cells versus WT aSyn; $\log_2$FC = 4.24, *padj* =2.52E-182 for control cells versus A30P aSyn]. FC scatter plots further confirmed that several genes were significantly deregulated in cells expressing WT aSyn, compared to control cells (Fig. 2A). An even more robust deregulation was observed in cells expressing A30P aSyn (Fig. 2A).

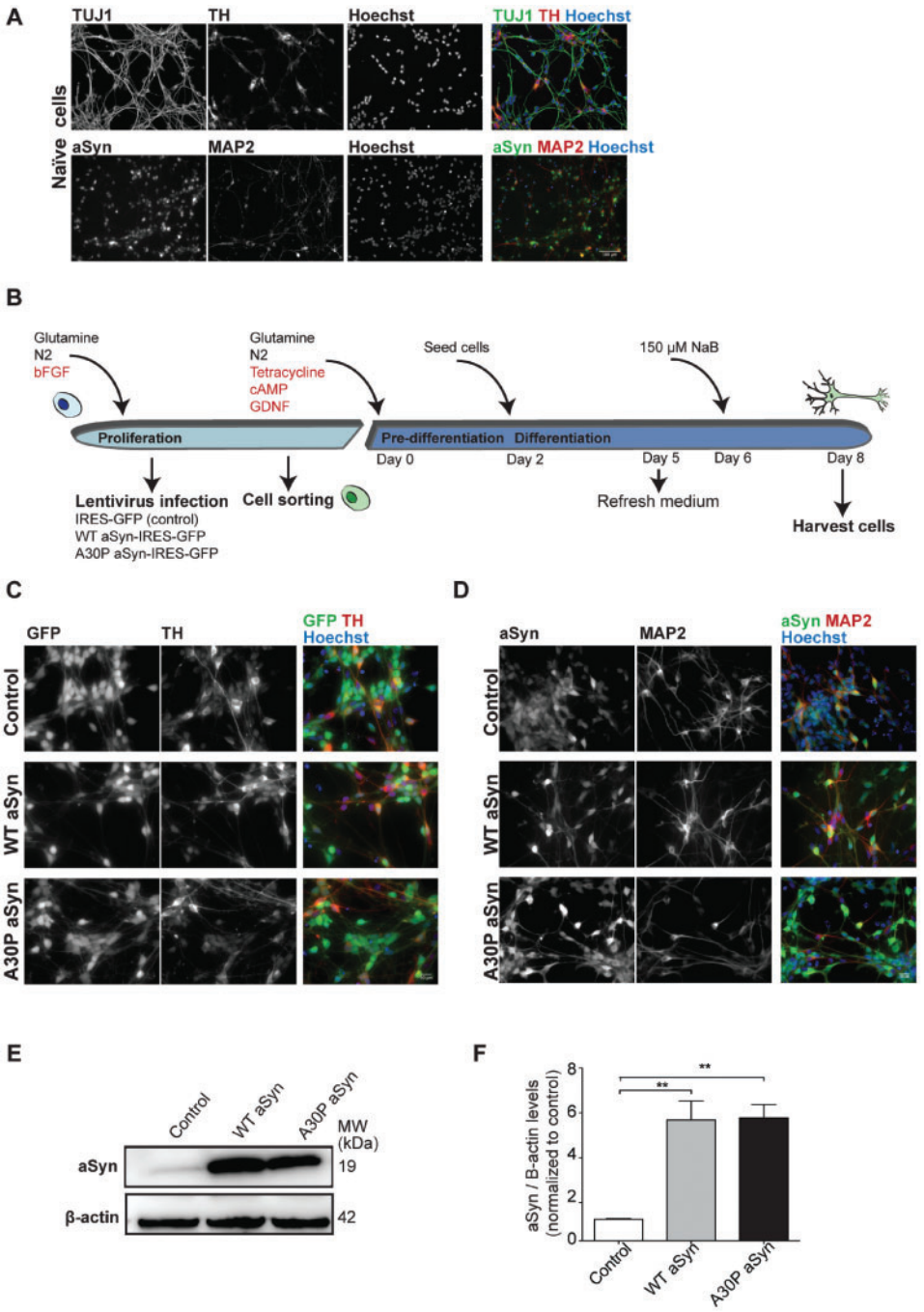

Figure 1. Study design and characterization of the three LUHMES cell lines used. LUHMES cells were differentiated as previously described [44]. Naïve cells grown on glass coverslips were immunostained for TUJ1, MAP2, TH or aSyn. Nuclei were stained with Hoechst. At day 8, differentiated cells exhibited an elaborate neurite network, strongly immunopositive for TH (**A**). Three cell lines were generated: control (IRES-GFP), WT, and A30P aSyn expressing LUHMES cells. Cells were treated according to the schematics and experiments were performed at differentiation day 8 (**B**). Differentiated LUHMES cells infected with viruses encoding for GFP, WT aSyn, or A30P aSyn, were immunostained for TH and co-stained with Hoechst. Images were acquired for each cell line showing highly homogeneous green-positive neuronal cells (**C**). aSyn was present both in the cell bodies and neurites, and stronger immunosignal was detected for WT and A30P aSyn cells (**D**). Immunoblot analyses were performed to assess the levels of aSyn protein in the three cell lines (**E**). Quantification of the immunoblot signals and immunostainings showed that WT and A30P aSyn expressing cells had significantly higher aSyn protein levels, compared to control cells (**F**). Data are expressed as mean ± SD of at least three replicates. One-way ANOVA, with Bonferroni correction, was used for statistical analysis with significance level of $P < 0.05$.

Considering $\log_2 FC > 0.5$ and $padj < 0.01$, we detected 647 downregulated genes and 355 upregulated genes in cells expressing WT aSyn. In cells expressing A30P aSyn, we found 813 downregulated and 657 upregulated genes. Analysis of differentially expressed genes (padj < 0.05) between control cells and those expressing WT aSyn showed a significant overlap to those deregulated between control and A30P aSyn expressing cells. In particular, we identified 710 upregulated and 914 downregulated genes in both conditions (Fig. 2B). Furthermore, we found distinct expression profiles when comparing WT aSyn to A30P

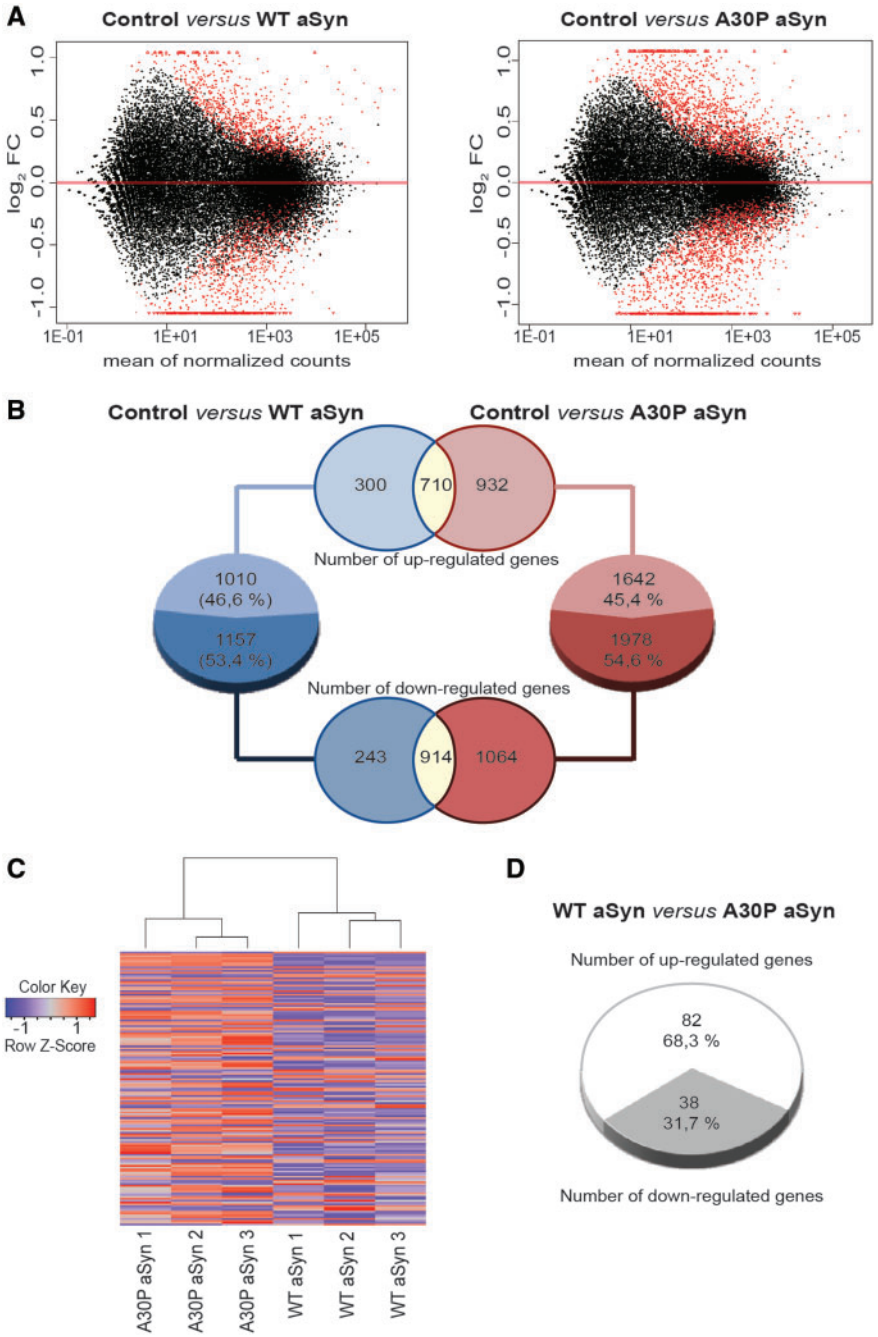

Figure 2. Gene expression changes associated with the expression of WT or A30P aSyn. (**A**) MA-plots were performed for differential gene expression data obtained when comparing RNA-seq data of cells expressing either WT or A30P aSyn. The log_2FC for each comparison is plotted on the y-axis and the average counts normalized by size factor is shown on the x-axis. The expression of aSyn promoted the differential expression of several genes with low expression levels. Each gene is represented with a dot. Genes with *padj* <0.01 are shown in red. (**B**) Pie-charts indicating the number of genes that are significantly (*padj* <0.05) up and downregulated upon expression of WT (blue) or A30P (red) aSyn, compared to control cells. Venn diagrams displaying the number of genes that are simultaneously upregulated (upper diagram) or downregulated (lower diagram) in both conditions. (**C**) Heatmaps of differentially expressed genes between WT and A30P aSyn. Color-spectrum codes the level of expression: blue color for low expression, and red color for high expression. Each column represents one independent experiment and each row one gene, in a total of 120 genes. (**D**) Pie chart showing how many genes are significantly up- and downregulated when comparing cells expressing WT aSyn versus A30P aSyn.

aSyn expressing cells (Fig. 2C). From a total of 120 differentially expressed genes, 82 were upregulated and 38 downregulated when comparing A30P aSyn to WT aSyn (Fig. 2D).

Consistently with previous studies (25), we observed that WT and A30P aSyn expression led to a significant reduction in the levels of NOTCH1. We also detected that NR4A2, the gene encoding Nurr1, was downregulated in both WT and A30P aSyn expressing cells, in agreement with other studies (12,26). However, the GDNF receptor alpha 2 was only significantly downregulated in cells expressing A30P aSyn. In these cells, we also detected significant downregulation of PRKCZ, but in contrast to previous reports (27), other members of the PRKC family, such as PRKCB (also known as Akt), PRKCE and PRKD1 where upregulated. Tyrosine 3-monooxygenase/tryptophan

5-monooxygenase activation protein eta (14-3-3θ), downregulated upon aSyn overexpression (28), was downregulated in cells expressing A30P aSyn. Importantly, downregulation of the dopamine receptor (DAT, SLC6A3), a putative early event in PD (29), was observed in LUHMES cells expressing either WT or A30P aSyn.

aSyn overexpression downregulates DNA repair genes

In order to determine the molecular pathways specifically affected by aSyn expression, we performed Ingenuity Pathway Analysis (IPA). The 500 most significant genes were used, rendering a *padj* cut off of 1.5E-3 for control versus WT aSyn, and of 1.6E-6 for control versus A30P aSyn. From the 500 genes, 156 were upregulated and 344 were downregulated in WT aSyn-expressing cells. Similar numbers were observed for A30P aSyn-expressing cells: 157 up- and 343 downregulated genes. IPA analysis revealed that a high number of differentially expressed genes were associated with 'cell cycle', 'DNA damage checkpoint', and 'ATM signalling' in cells expressing WT or A30P aSyn (Fig. 3A and B).

Next, we performed additional network analysis of differentially deregulated genes using ToppGene Suite (Supplementary Material, Table S3). Upregulated and downregulated genes were analysed separately. Consistently with IPA analysis, the main biological processes downregulated upon expression of WT or A30P aSyn were 'cell cycle' and 'cellular response to DNA damage stimulus' (Supplementary Material, Table S3). On the other hand, analysis of upregulated pathways revealed differences between cells expressing WT and A30P aSyn: WT aSyn induced upregulation of genes involved in mitochondrial energy metabolism, whereas A30P aSyn induced upregulation of genes linked with neuron differentiation and synaptic transmission.

The effect of aSyn on DNA-repair associated genes was further corroborated by gene ontology analysis using David Functional Annotation database (Supplementary Material, Table S4). Protein association network analysis of genes involved in DNA repair, using STRING, revealed a strong interaction between DNA-damage response molecules (Fig. 4A and B). A large number of DNA repair-associated genes was downregulated in both WT and A30P aSyn expressing cells (genes in red), whereas, approximately, one-third of the genes were exclusive to one of the conditions. Three of the most downregulated DNA repair-associated genes (BRCA2, TOP2A and FOXM1) were selected for further validation by real-time PCR (qPCR). Differential expression analysis from the RNA-seq results showed that TOP2A exhibited the strongest downregulation in both WT (Fig. 4C) and A30P aSyn expressing cells (Fig. 4D). The analysis by qPCR confirmed a significant downregulation of these genes in cells expressing WT aSyn, but only a trend, that did not reach significance, for BRCA2 and FOXM1 in A30P aSyn cells (Fig. 4E).

WT, but not A30P aSyn, induces DNA damage and impairs miROS handling in dopaminergic neurons

To investigate whether WT and A30P aSyn promoted DNA damage, we performed comet assay analysis in order to detect DNA single-strand breaks, double-strand breaks, and alkali-labile lesions. Tail moment analysis demonstrated that cells expressing WT aSyn displayed the highest tail moment compared to control and those expressing A30P mutant (Fig. 5A and B). To further characterize the DNA damage induced by aSyn, we assessed the levels of phosphorylated H_2AX (p-H_2AX) and phosphorylated p53 (p-p53) using immunoblot analyses. Consistently, we found that only cells expressing WT aSyn displayed increased levels of p-p53 compared to the cells. Curiously, no significant changes were observed in the levels of p-H_2AX (Fig. 5C and D).

Damage of genomic DNA may occur in the presence of high levels of reactive oxygen species (ROS) (30). Thus, we asked whether the DNA damage was associated with the levels of mitochondrial ROS (miROS). Using MitoSOX probe, we found no differences between the three cell lines at basal levels. Thus, we investigated whether stressing the cells with 5% H_2O_2, as a 'second hit', would unbalance cells and expose differences in ROS handling. Indeed, 30 min after exposure to H_2O_2, cells expressing WT aSyn showed a significant increase in miROS production compared to control. No significant differences were detected for cells expressing A30P aSyn (Fig. 5E). To assess overall redox changes in the cell, we quantified the levels of oxidized 2′,7′-dichlorofluorescein diacetate (DCFDA). No significant differences were observed between the three cell lines (Fig. 5F), suggesting the effect was stronger at the level of mitochondria. Since mitochondria are key modulators of apoptotic pathways, we investigated the impact of aSyn on the activation of caspase 3, a key player in apoptosis. We found that both the WT and A30P aSyn significantly increased the percentage of cells immunopositive for cleaved caspase 3 (Fig. 5G). Interestingly, we found no significant differences in cytoplasmic membrane integrity between the three cell lines, suggesting that miROS alterations and activation of apoptosis may be early effects of increased levels of expression of WT aSyn, which do not directly result in strong cytotoxicity (Fig. 5H).

Sodium butyrate alleviates WT aSyn-induced DNA damage

It has been suggested that aSyn may impact on gene transcription via modulation of acH3. Thus, we next investigated the levels of acH3 in whole cell lysates (Fig. 6A). Immunoblot analysis demonstrated a highly significant reduction in the levels of acH3 in cells expressing WT aSyn. A milder, but also significant, effect was observed in cells expressing A30P aSyn (Fig. 6B). We then asked whether modulation of histone deacetylase activity, using NaB, would revert the reduction in the levels of acH3 induced by aSyn. After determining the optimal concentration of NaB (150 μM, Fig. 6C), we treated the three cell lines with the compound for 48 h and observed an increase in the levels of acH3 levels in the presence of aSyn, but only significant in the presence of the WT aSyn (Fig. 6D and E).

Given the strong effect observed, we then asked whether NaB could rescue cells from DNA damage induced by aSyn, and performed comet-assay analysis. NaB treatment led to a reduction on tail moment values in all the conditions, but the effect was particularly striking in WT aSyn LUHMES cells (Fig. 7A and B). Additionally, we also found a significant reduction in the levels of p-p53 in cells expressing WT aSyn (Fig. 7C and 7D), and a reduction in miROS, compared to the control cells (similar to Fig. 7E).

Next, to assess whether the protective effects of NaB would derive from modulation of gene expression, we investigated the levels of the three DNA-repair genes selected above using qPCR. Strikingly, we verified that NaB restored FOXM1 and BRCA2 expression levels in cells expressing WT aSyn. Curiously, the levels of FOXM1 in cells expressing WT aSyn and treated with NaB

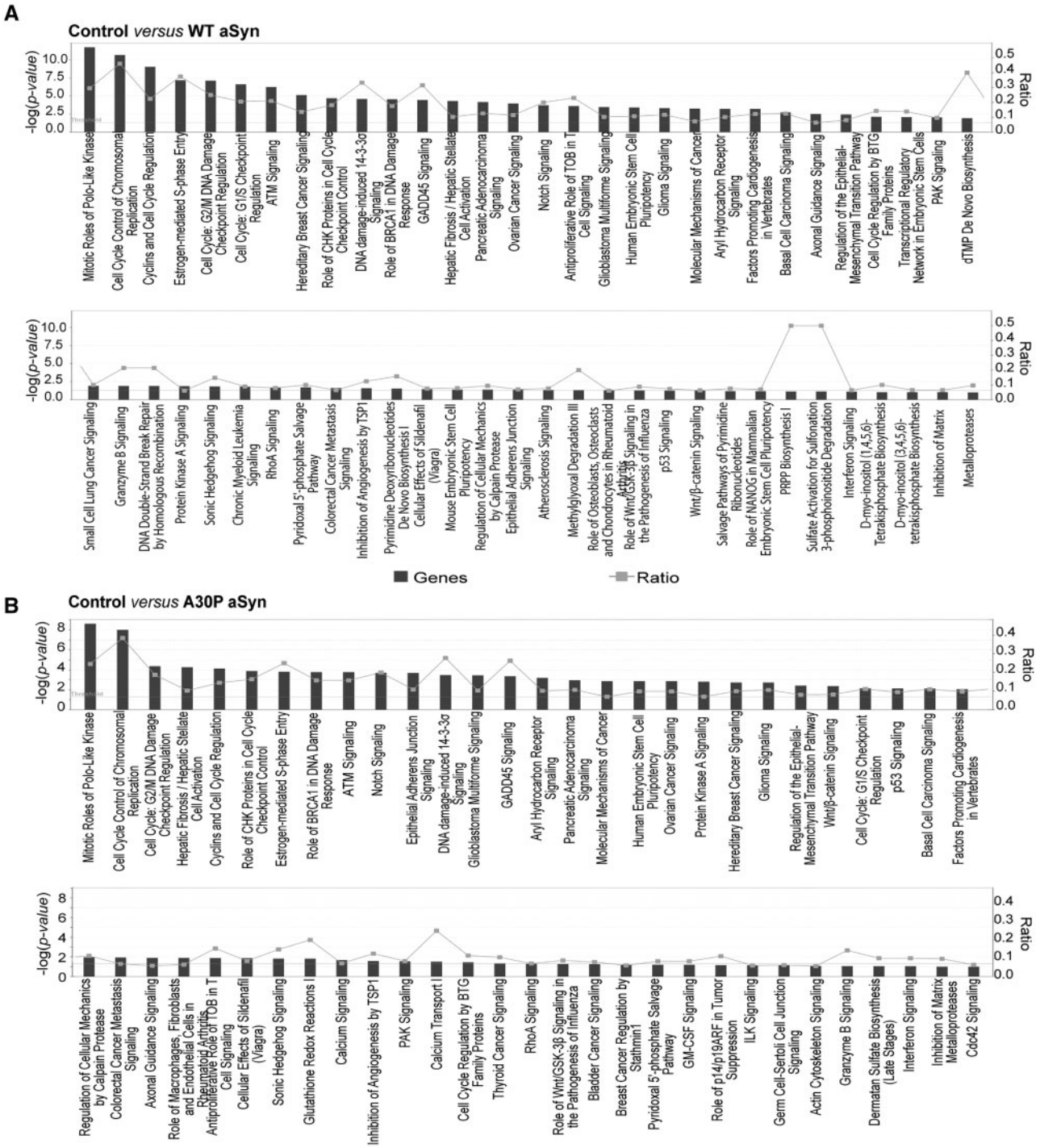

Figure 3. Ingenuity pathway analysis (IPA) of RNA-seq data comparing gene expression profiles of cells expressing WT or A30P aSyn. IPA graphs showing the predominant canonical pathways of differentially expressed genes in cells expressing the WT (**A**) or A30P (**B**) aSyn, compared to control cells. The ratio (gray line) indicates the number of genes within each pathway divided by the total number of genes in the canonical pathway. IPA showed that both WT and A30P aSyn impacts the expression of genes associated with a multitude of pathways, suggesting a pivotal role of aSyn in the expression of genes associated with cell cycle and DNA damage checkpoints.

were significantly higher than those in cells expressing A30P aSyn. Although we found also increase in the levels of TOP2A upon NaB treatment, this did not reach significance. The apparent increase in the levels of TOP2A upon NaB treatment in cells expressing WT or A30P aSyn did not reach statistical significance; indeed, the only significant effect was the reduction in TOP2A levels in control cells, suggesting there might have been a protective effect in cells expressing aSyn (Fig. 7F).

Finally, to assess the overall protective effect of NaB on cellular pathologies associated with PD, we used a different model based on the treatment of naïve LUHMES cells with the neurotoxin 1-methyl-4-phenylpyridinium (MPP^+), a known inducer of

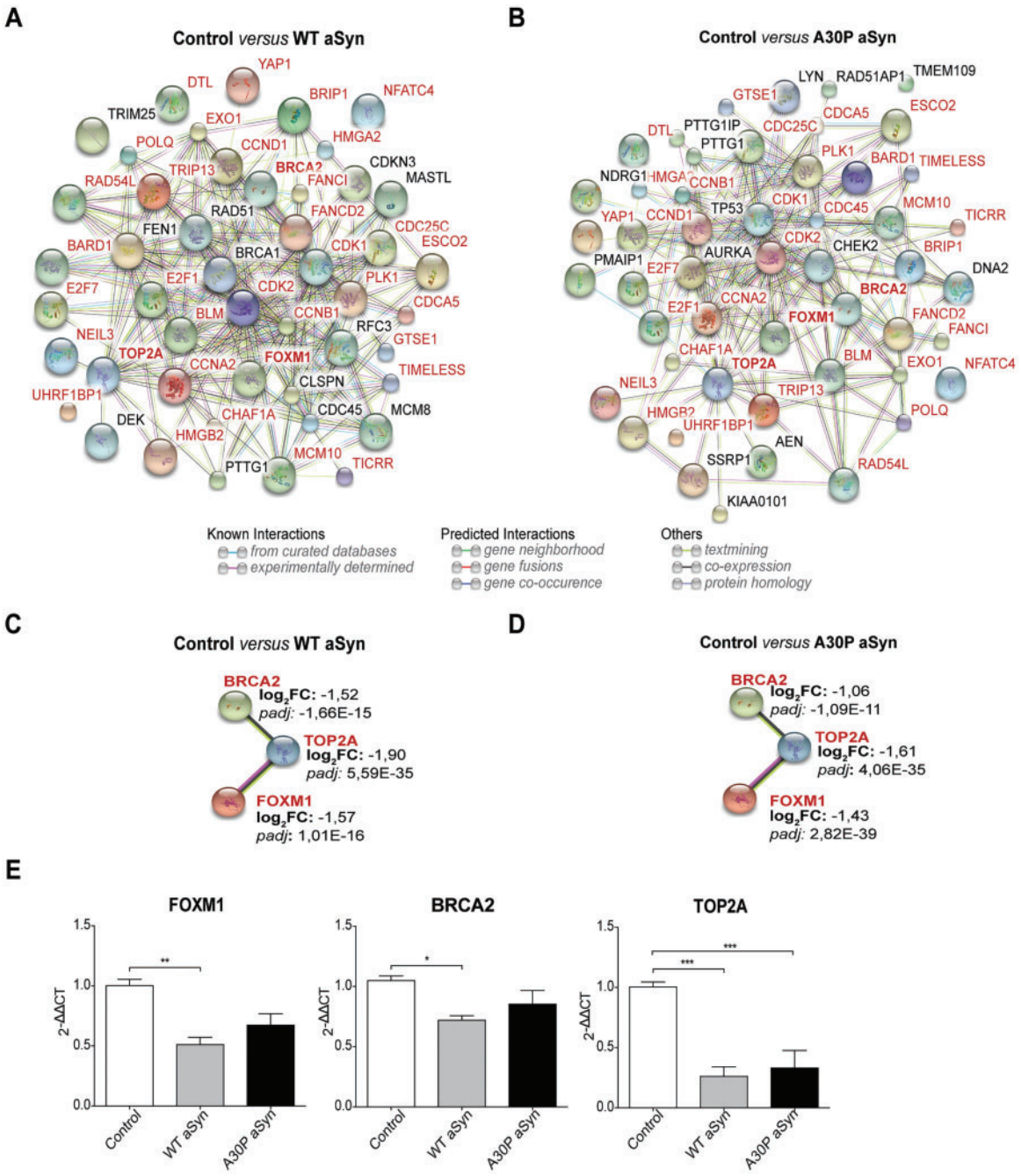

Figure 4. Downregulation of DNA repair-associated genes in dopaminergic cells expressing WT or A30P aSyn. STRING protein network analysis of DNA repair genes downregulated in WT (**A**) or A30P (**B**) expressing cells, compared to control cells. Approximately two-thirds of the genes are deregulated in both conditions (genes in red). Genes exhibiting highly significant downregulation in WT (**C**) and A30P (**D**) aSyn expressing cells were selected for qPCR validation (**E**). qPCR analysis confirmed a strong deregulation of TOP2A in both WT and A30P aSyn expressing cells, while FOXM1 and BRCA2 were only significantly downregulated in cells expressing WT aSyn. Data are expressed as mean ± SD of at least three replicates. One-way ANOVA, with Bonferroni correction, was used for statistical analysis with significance level of $P < 0.05$.

cellular changes characteristic of PD, including oxidative stress and DNA fragmentation (31). Importantly, we confirmed the protective effects of NaB in naïve LUHMES cells treated with MPP^+. Since the toxin is known to induce strong gene expression changes, we focused on the rescue of cytotoxicity. TUJ1 staining revealed a strong rescue of neurite integrity (Supplementary Material, Fig. S1A), and of membrane integrity, as measured by the adenylate kinase (AK)-release assay (Supplementary Material, Fig. S1B), upon NaB treatment in cells exposed to MPP^+.

Discussion

Our study provides new evidence for a role of aSyn on transcription deregulation in dopaminergic cells, and uncovers new pathways underlying aSyn toxicity. Both WT and A30P aSyn

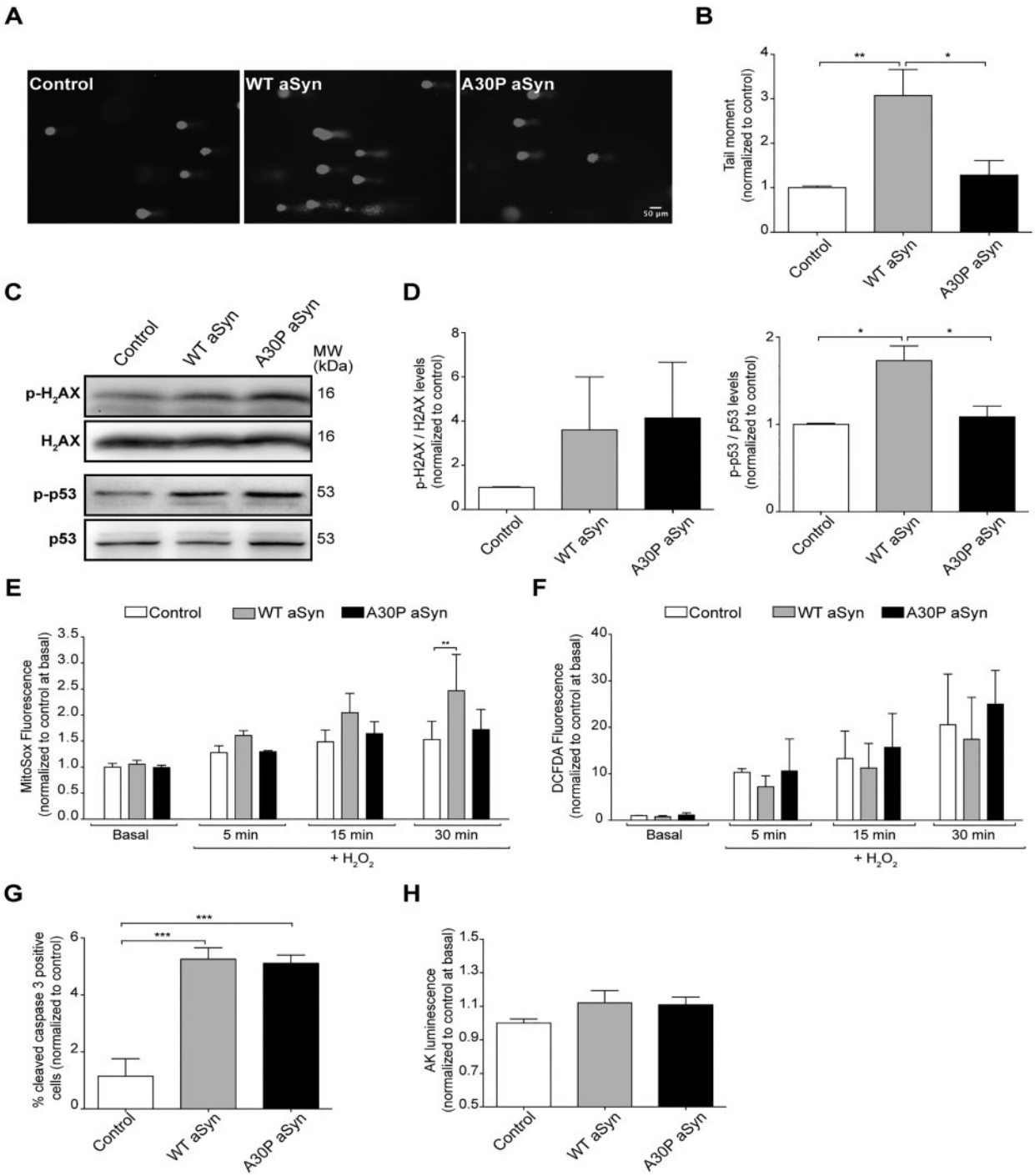

Figure 5. WT aSyn induces DNA damage and impairs miROS handling. The comet assay alkali method was used to detect DNA single-strand breaks, double-strand breaks, and alkali-labile lesions. Following PI staining, comets were imaged using epifluorescence microscopy. Representative images are presented for each condition (**A**). Tail moments were calculated using the Comet Score software. Statistical analysis showed that tail moments from cells expressing WT aSyn were significantly higher than in control or A30P aSyn expressing cells (**B**). Levels of p-H2AX and p-p53 were analysed by immunoblot analyses (**C**). Quantification of the immunoblots confirmed a trend towards an increase of p-H2AX levels, and a significant increase in the levels of p-p53 (**D**). miROS were measured using MitoSOX Red. At basal levels, no differences in miROS between the three cell lines were observed. About 30 min after treatment with 5% H_2O_2, miROs levels were significantly higher in LUHMES cells expressing WT aSyn (**E**). Similar experiments performed with DCFDA revealed no significant differences in the total cellular levels of ROS (**F**). The percentage of cleaved caspase 3 immunopositive cells was calculated. (**G**). Bioluminescence measurement of AK performed with Toxilight assay showed no differences in cytotoxicity between the cell lines (**H**). Data are expressed as means ± SD of at least three replicates. One-way ANOVA (B and D) or two-way ANOVA (E and F), with Bonferroni correction, was used for statistical analysis with significance level of $P < 0.05$.

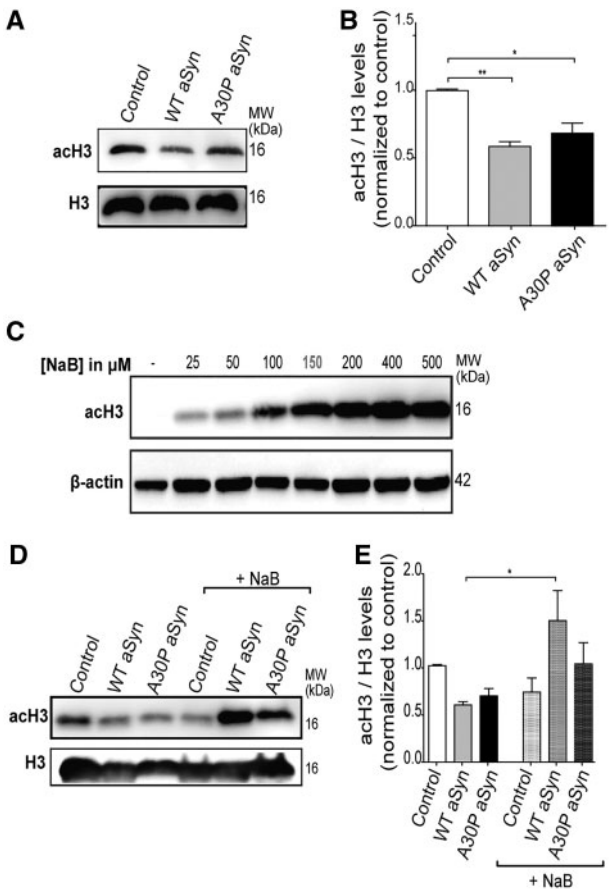

Figure 6. aSyn-mediated reduction in the levels of acH3 is rescued NaB. An evident reduction of acH3 levels (lysine 9) was observed in cells expressing either WT or A30P aSyn (**A**). Quantification of the immunoblots revealed a significant decrease of acH3 levels in cells expressing the WT aSyn, and a more modest, although still significant, reduction in cells expressing A30P aSyn (**B**). acH3 levels were assessed in cells treated with different concentrations of NaB, for 48 h. An evident increase in acH3 levels was already observed for cells treated with 150 µM NaB (**C**). The three cell lines exhibited higher levels of acH3 upon treatment with 150 µM NaB for 48 h (**D**). This effect was particularly strong in cells expressing WT aSyn (**E**). Data are expressed as mean ± SD of at least three replicates. One-way ANOVA, with Bonferroni correction, was used for statistical analysis with significance level of $P < 0.05$.

downregulated the expression of genes involved in DNA repair, which we suggest may be an early indication of toxicity promoted by aSyn. Interestingly, we identified effects induced by WT aSyn but not by the A30P mutant, underlining their distinct biochemical and biological properties (Fig. 8A–F). Finally, we demonstrated that treatment with the general HDACi NaB ameliorated aSyn-induced transcription deregulation and prevented DNA damage (Fig. 8G and H).

The interplay between transcription deregulation and neurodegenerative diseases has been a subject of interest in the last decade (7,32,33). However, the involvement of aSyn on transcription was only recently suggested (4,5). Through RNA-seq analyses of dopaminergic LUHMES cells infected with viruses encoding for either WT or A30P mutant aSyn, we evaluated the impact of these aSyn variants on transcription. We observed a distinct and highly significant transcription deregulation in aSyn expressing cells. Our results are in line with previous findings, where genes such as NR4A2 (12,26), NOTCH1 (34) and 14-3-3θ (28) were identified. However, we now identify novel pathways that shed new light into our understanding of the effects of aSyn on gene expression. In our dopaminergic cell model, most downregulated genes were involved in cell cycle and DNA repair. Two previous studies reported that aSyn can act as a cell cycle regulator (35) and is an important player on the initiation of DNA replication (18). A close link between unrepaired DNA damage and neurodegeneration process was recently suggested (36,37). Although mitochondrial impairment and oxidative stress are common causes of DNA damage in neurons, deregulation of DNA repair genes may constitute the tipping point. In Alzheimer's Disease, p53 and BRCA1, a crucial gene in DNA repair that was also downregulated in our WT aSyn cells, have been recently put forward as central players in the disease pathogenesis and are now considered promising therapeutic targets (38). In PD, mutations in ATM, a gene encoding for an important protein involved in DNA repair, are a risk factor (39). Interestingly, we have also recently discovered that alterations in DNA repair genes may be linked to PD progression (7). Last year, it was also shown that Ercc1 deficient mice, having impaired DNA excision repair, displayed typical PD-like pathological alterations, such as decreased striatal dopaminergic innervation, defects in mitochondrial respiration, and increased levels of phosphorylated aSyn (40). In differentiated neuroblastoma cells, aSyn expression led to increased DNA damage upon exposure to Fe(II) (41). However, to the best of our knowledge, aSyn has not been previously associated with transcriptional deficits on DNA repair genes.

We selected three major genes involved in DNA repair (FOXM1, BRCA2 and TOP2A), and validated the expression changes observed in the RNA-seq experiments by qPCR. Consistently, the expression levels of all three genes were significantly lower in cells expressing WT aSyn. In cells expressing A30P aSyn, the expression of TOP2A was significantly lower, but for FOXM1 and BRCA2 we observed only a slight downregulation. We then used a combination of established reporters for DNA damage to understand how aSyn-induced transcription deregulation impacts on cell viability and, specifically, on DNA damage. Increased tail-moment values, measured via comet assay (42), and p-p53 levels confirmed DNA damage in cells expressing WT aSyn. Surprisingly, we did not detect a significant increase on p-H_2AX levels, suggesting that H_2AX-independent DNA damage mechanisms might be taking place.

aSyn is involved in mitochondrial dysfunction, a molecular mechanism implicated in the onset and progression of PD (43,44). Although the localization of aSyn in mitochondria is still not consensual, overexpression of aSyn promotes several mitochondrial abnormalities, including decreased complex I activity and unbalanced miROS handling, resulting in increased oxidative stress and activation of apoptosis (45–48). The nuclear genome is susceptible to damage by increased levels of ROS generated during mitochondrial respiration or due to exposure to exogenous toxins (30). While we did not observe differences in total ROS levels, we detected a significant increase of miROS in cells expressing WT aSyn treated with H_2O_2, suggesting that aSyn causes impairs the handling of ROS species, specifically at the mitochondrial level. Although it is possible that other mechanisms also play a role in aSyn-induced DNA damage, the impact of aSyn on miROS handling may be a major culprit in this process. Future studies, addressing the effect of both WT and mutant aSyn on mitochondrial homeostasis and morphology, will be important to elucidate the mechanisms associated with the impact of aSyn on mitochondrial biology.

In the event of increased DNA damage (e.g. due to increased oxidative stress), the preferred survival strategy of a cell is to

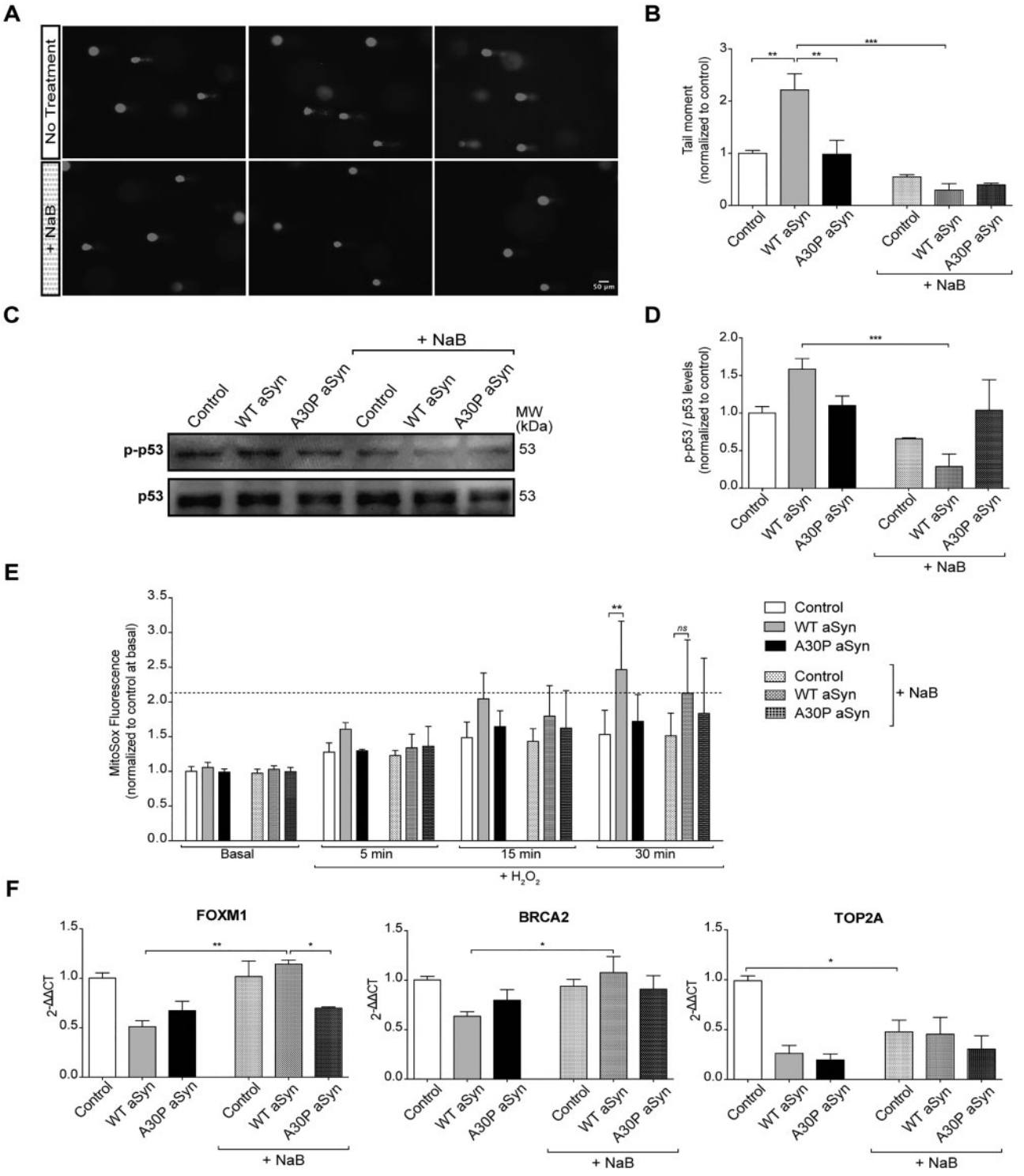

Figure 7. NaB rescues the DNA damage induced by WT aSyn expression. Representative images of comets obtained using the alkaline comet assay are shown for each condition (**A**). Comet assay analysis showed a significant decrease in tail moment in cells expressing WT aSyn after treatment with 150 µM of NaB (**B**). Levels of p-p53 were measured using immunoblot analysis (**C**). Quantification of the immunoblots showed a reduction in the levels of p-p53 in WT aSyn expressing cells treated with NaB (**D**). Assessment of miROS using MitoSOX Red indicated that the levels of miROS in cells expressing WT aSyn treated with H_2O_2 were reduced upon treatment with 150 µM NaB (**E**). qPCR analysis of DNA repair-associated genes upon treatment with 150 µM NaB showed the normalization of the expression FOXM1 and BRCA2 in cells expressing WT aSyn (**F**). Data are expressed as mean ± SD of at least three replicates. One-way ANOVA (B, C and E) or two-way ANOVA (E and F), with Bonferroni correction, were used for statistical analysis with significance level of $P < 0.05$.

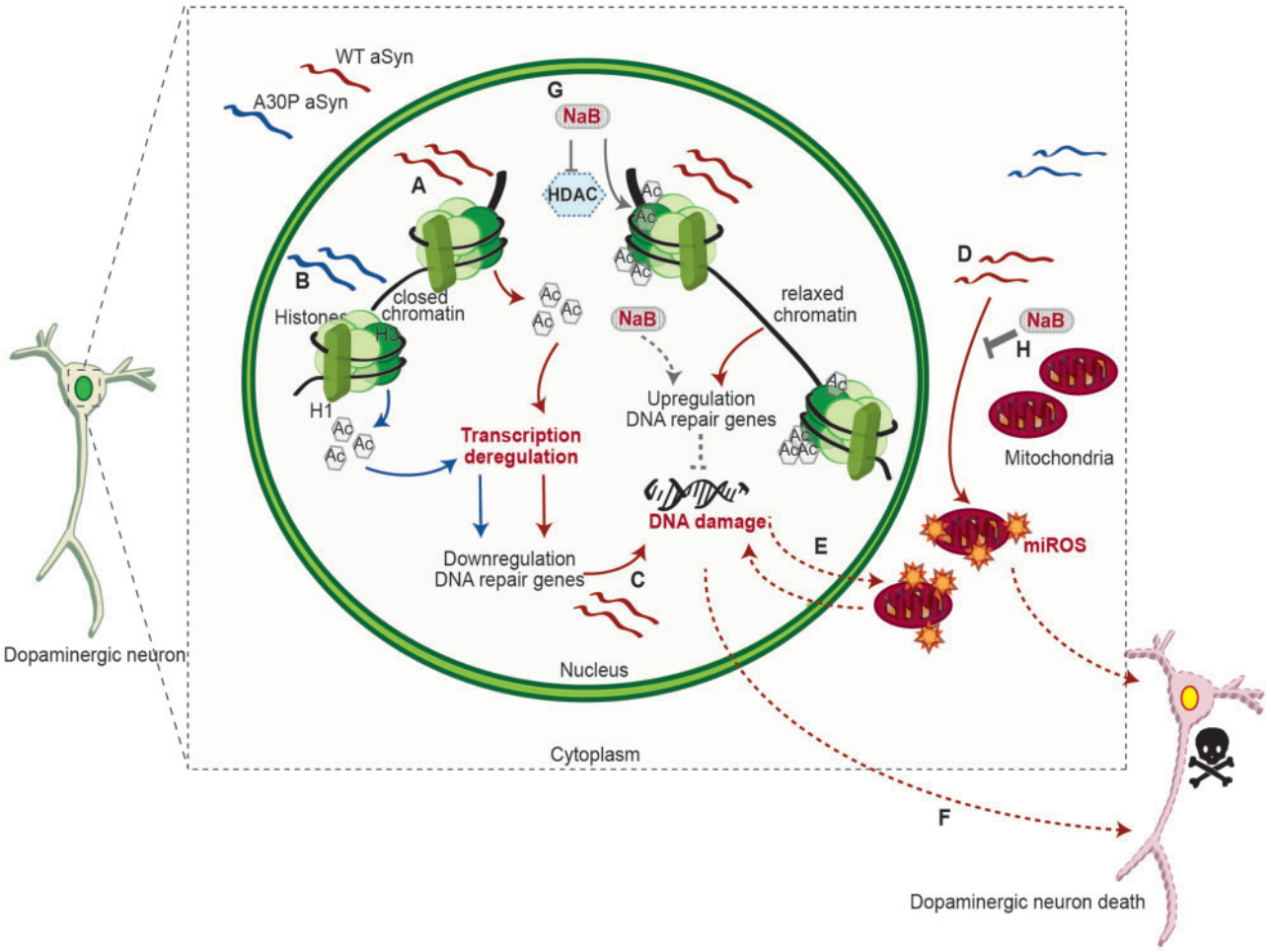

Figure 8. Proposed model for the neurotoxicity associated with increased levels of expression of aSyn in dopaminergic cells. Increased levels of WT (**A**) or A30P aSyn (**B**) reduce the levels acH3. H3 hypoacetylation causes chromatin condensation and transcription repression. Thus, we propose that altered acH3 levels may be, at least partially, involved in the transcriptional deregulation mediated by WT (**C**) or A30P aSyn (**D**) in dopaminergic neurons. Gene expression analysis revealed downregulation of genes involved in DNA repair in cells expressing both aSyn variants. Interestingly, our data indicate that only WT aSyn promotes DNA damage in these neuronal cells (**C**), highlighting a distinct biological effect of the two aSyn variants. Although several mechanisms may underlie these differences, the negative impact of WT aSyn on mitochondrial ROS handling (**D**) represents an additional source of DNA damage (**E**). We propose that these alterations may be early effects of increased levels of WT aSyn (**F**). Excitingly, increasing acH3 levels, via NaB treatment, rescued dopaminergic neurons from WT aSyn-induced DNA damage and restored the expression levels of specific DNA repair genes (**G**). In addition to the effect on transcription, NaB improved the handling of ROS (**H**), which further contributes to alleviate the neurotoxic effects promoted by WT aSyn.

activate cell cycle arrest and a complex set of DNA repair pathways (49). However, as WT aSyn leads to a downregulation of DNA repair genes, damage to DNA becomes excessive and, ultimately, may lead to apoptosis. Consistently with previous reports showing that aSyn overexpression activates apoptosis (48,50), we found an increase in the percentage of cells that are positive for cleaved caspase 3. Interestingly, activation of apoptosis was also induced in cells expressing A30P aSyn, although no changes in DNA integrity and miROS species handling were detected. However, the A30P aSyn mutant displays different biochemical properties than WT aSyn, such as differential affinity to bind membranes (51), and reduced cytotoxicity in yeast models (52), producing distinct effects on cells. Our results confirm the idea that aSyn mutants might affect cellular homeostasis via distinct mechanisms. On the other hand, since mitochondria are key modulators of apoptosis (53), these results further corroborate the hypothesis that, at least in our model, aSyn may impact mitochondrial function. Future studies will be necessary to further understand whether other mechanisms are underpinning aSyn-induced DNA damage and toxicity.

Importantly, we did not observe significant alterations in cytoplasmic membrane integrity upon aSyn expression. This suggests that transcriptional deregulation and DNA damage may be early events in the cascade of aSyn-induced neurotoxicity, which helps us delineate the order of the cascade of events involved.

We then investigated how aSyn promotes transcription deregulation and whether it could be reversed, as this would have strong interest for therapeutic purposes. aSyn was previously shown to interact with DNA (14) and to regulate acH3 levels (17–19). Post-translational modifications of histones are essential in the regulation of transcription activation/repression, DNA replication, and repair of DNA damage (20). Consistently with previous findings (19), we found that increased levels of aSyn significantly reduce the levels of acH3. This effect was particularly strong in cells expressing WT aSyn. This prompted us to

test whether increasing acH3 levels, using HDACi, could be a useful strategy for mitigating aSyn-induced cellular pathologies. Intriguingly, the effect of NaB on acH3 levels were only significant in WT aSyn-expressing cells, suggesting that the mechanism of action may be different than that observed in cells expressing A30P aSyn. The beneficial effects of HDAC inhibition are still controversial, as both neuroprotective (22) and neurotoxic (23) effects were reported. NaB is a short chain fatty acid that preferentially affects HDACs from classes I and IIa and other non-histone targets.

Our study showed that treatment of dopaminergic cells expressing WT aSyn with NaB strongly reduces DNA damage, as assessed by comet assay and levels of p-p53. We also observed a reduction in the levels of miROS. Interestingly, previous studies showed mitochondrial function improvement upon treatment with NaB in Huntington's disease models (54).

In the context of cancer, HDACi are used to promote DNA damage through transcription downregulation, impairment of DNA repair proteins, and increase in oxidative stress. In contrast, HDACi confer protection against oxidative stress in neuronal cells (20,21). In our model, in addition to the effect on miROS handling, NaB appears to modulate the transcription of genes involved DNA repair. When we evaluated the expression of major genes involved in DNA repair, we found that protection by NaB involves the restoration of the levels of expression of DNA repair genes, including FOXM1 and BRCA2. Interestingly, the effect of NaB on FOXM1 was significantly stronger in WT aSyn versus A30P aSyn-expressing cells, further corroborating our hypothesis that NaB may act via distinct mechanisms on cells expressing WT and A30P mutant aSyn. Altogether, these findings suggest that WT aSyn may cause transcriptional deregulation and cytotoxicity via chromatin remodeling, and that this can potentially be rescued by increasing histone acetylation levels (eg. treatment with HDACi). On the other hand, although A30P aSyn also promotes histone 3 hypoacetylation, it is likely that other molecular events are also associated with its cytoxicity.

Given the beneficial effects of NaB on aSyn-mediated DNA damage, we asked whether this compound was also protective on a distinct model of PD, also characterized by mitochondrial impairment, increased oxidative stress and DNA fragmentation (31). Importantly, we observed a clear neuroprotective effect of NaB in naïve LUHMES cells exposed to the neurotoxin MPP^+.

In conclusion, although several questions demand additional investigations, we provide novel evidence suggesting that transcriptional deregulation and nuclear DNA damage are connected with the toxicity of increased levels of aSyn in dopaminergic cells, opening novel avenues for the development of future intervention strategies in PD.

Materials and Methods

Cell culture

LUHMES cells were maintained and differentiated as previously described (24). Briefly, cells were cultured in flasks (Corning) pre-coated with 50 μg/mL poly-L-ornithine and 1 μg/mL fibronectin (Sigma–Aldrich), and grown at 37°C in a humidified 5% CO_2 atmosphere. Advanced Dulbecco's modified Eagle's medium/F12 (DMEM/F12, Gibco) supplemented with 1× N2 (Gibco), 2 mM L-glutamine (Gibco) and 40 ng/mL recombinant basic fibroblast growth factor (bFGF, R&D Systems) was used to maintain proliferating LUHMES cells. Differentiation was achieved by replacing the proliferating medium with DMEM/F12 supplemented with 1× N2, 2 mM L-glutamine, 1 mM dibutyryl cAMP (cAMP, Sigma Aldrich), 1 μg/mL tetracyclin (Sigma–Aldrich) and 2 ng/mL recombinant human GDNF (R&D Systems). Two days after adding differentiation medium, cells were trypsinized [(138 mM NaCl, 5.4 mM KCl, 6.9 mM NaHCO3, 5.6 mM D-Glucose, 0.54 mM EDTA, 0.5 g/L trypsin from bovine pancreas type-II-S (Sigma–Aldrich)] and seeded into poly-L-ornithine/fibronectin pre-coated plates (Corning) or glass coverslips. On day 5, one-third of the medium was refreshed. Experiments were performed 8 days after differentiation. A schematic representation of the overall differentiation process is provided on Figure 1A.

Generation of aSyn expressing LUHMES cells

Full-length human aSyn c-DNA (*SNCA*, NM_000345) or A30P aSyn were subcloned into a second generation bicistronic lentiviral vector, pWPI (Tronolab, Switzerland), under the chicken/β-actin (CBA) promoter. All cloned sequences were verified by direct-sequencing (StarSeq). pWPI vector containing only IRES-GFP cassette was used as infection control in all the experiments. Second-generation lentiviral particles were generated as previously described (55). Briefly, 293T cells were transiently co-transfected with the modified transfer vector plasmids and second-generation packing system (Tronolab). Supernatant was collected 48-h post-transfection, concentrated by PEG-it Virus Precipitation Solution (System Bioscience) and resuspended in Panserin 402 (PAN). Lentiviral vector titers were quantitatively measured by qPCR using primer sequences specific for the woodchuck hepatitis virus post-transcriptional regulatory element (WPRE), as previously described (56). To generate cells expressing aSyn, proliferating LUHMES cells were infected with equimolar amounts of IRES-GFP, WT aSyn-IRES-GFP or A30P aSyn-IRES-GFP lentivirus. Positive green fluorescent cells were selected by fluorescence activated cell sorting (Calibur flow cytometer, BD Biosciences).

Sodium butyrate treatment

The concentration of NaB (Sigma) was determined by treating differentiated LUHMES cells with increasing concentrations (0–500 μM) of the drug. NaB was dissolved in DMEM/F12 medium and added to LUHMES cells on differentiation day 6, for 48 h. On differentiation day 8, cells were harvested for western-blot analysis of acH3 levels. For subsequent experiments, cells were treated on day 6 with 150 μM NaB (Fig. 1A), as it represented the lower NaB concentration leading to a high increase of H3 acetylation.

Treatment with MPP^+

LUHMES cells were treated with 2.5 μM MPP^+, dissolved in water, on day 5 of differentiation. Subsequent experiments were performed 3 days after starting the treatment (Fig. 1A).

Cytotoxicity assay

Cell viability was assessed by quantitatively measuring AK content in the supernatants of cells. ToxiLight bioassay kit (Lonza) was used according to the manufacture recommendations.

Immunocytochemistry

Cells on coverslips were fixed with 4% paraformaldehyde, for 15 min, at room temperature (RT). About 1× saline phosphate

buffer (PBS) was used to wash the cells before permeabilization with 0.5% Triton/PBS, for 15 min at RT. After blocking with 3% BSA/PBS for 1 h at RT, cells were incubated, overnight at 4°C with primary antibodies diluted in blocking solution: anti-TUJ1 1:3000 (Covance, mouse); anti-TH 1:1000 (Millipore, rabbit); anti-MAP2 1:1000 (Abcam, rabbit), anti-aSyn 1:2000 (BD Transduction, mouse) and anti-cleaved caspase 3 1:2000 (Cell Signaling). Cells were washed with 1× PBS before incubation with secondary Alexa Fluor antibodies (rabbit or mouse, 488 or 555, Life Technologies), prepared at 1:10 000 in blocking buffer, for 2 h at RT. Before mounting the coverslips with Moviol, nuclei were stained with Hoechst. Immunofluorescence images were acquired using an epifluorescence microscope (Leica DMI 6000B microscope, Leica). To assess the percentage of cells displaying cleaved caspase 3, images were acquired on Olympus IX81-ZDC microscope system, using a 40× magnification objective. The percentage of cleaved caspase 3 positive cells was calculated based on the total number of cells (DAPI). For each cell line, at least 150 cells ($N \geq 167$) were counted from seven or eight different optical fields. Cells were manually counted using Image J software. The relative amount of cleaved caspase 3 positive cells was calculated by normalizing to control cells expressing GFP.

Western blot

For protein analysis, differentiated LUHMES cells were incubated with RIPA buffer [0.1% Triton X-100, 0.15 M NaCl, 50 mM Tris pH 7.5 and a protease inhibitor cocktail tablet (Roche)], on ice, for 30 min. Lysates where then collected, sonicated on ice for 10 s at 40–50% power, and centrifuged at 14 000 rpm for 30 min, at 4°C. Protein concentration was determined using the Bradford assay (BioRad), in an Infinite M200 PRO plate reader (Tecan Lta). Total lysates (40–60 µg) were mixed with 5× Laemmli buffer (250 mM Tris pH 6.8, 10% sodium dodecyl sulfate, 1.25% Bromophenol Blue, 5% β-mercaptoethanol, 50% glycerol), boiled at 95°C for 5 min, and loaded on 12% sodium dodecyl sulfate polyacrylamide (SDS–PAGE) gels. After electrophoresis, proteins were transferred on a Trans-blot Turbo system to either nitrocellulose or PVDF membranes (Trans-blot Turbo Nitrocellulose/PVDF membranes, BioRad). About 5% skim milk, prepared with 1× Tris Base Solution/0.05% Tween (TBST), was used for blocking. After 1 h at RT, membranes were incubated overnight at 4°C with primary antibodies diluted in 4% BSA/TBST. The following antibodies and dilutions were used: anti-aSyn 1:2000 (BD Transduction, mouse); anti-p-p53 Ser46 1:1000 (Cell Signalling, rabbit), anti-p53 1:1000 (Cell Signalling, rabbit); anti-p-H_2AX 1:1000 (Cell Signalling, rabbit); anti-H_2AX 1:1000 (Cell Signalling, rabbit); anti-acH3K9 1:2000 (Millipore, rabbit); anti-H3 1:5000 (abcam, rabbit) and β-actin 1:5000 (Sigma, mouse). Membranes were then incubated with horseradish peroxidase-conjugated secondary antibodies 1:10 000 (mouse or rabbit, GE Healthcare), for 2 h at RT. Between steps, membranes were washed 3 times with TBST, for 5 min at RT. Chemiluminescent signals on the blots were detected using Immobilon Western Chemiluminescent HRP Substrate (Millipore Corporation) and Fusion FX (Vilber Lourmat). Quantification of bands was performed using Image J software.

RNA extraction

Total RNA from differentiated LUHMES cells was extracted and purified using the RNeasy mini kit (Qiagen), according to the instructions of the manufacturer. Three biological replicates were used for RNA-seq experiments. Sequencing and RNA quality analysis was performed as described previously (57). In brief, RNA quality was assessed using RNA 6000 Nano chips run on a 2100 Bioanalyzer (Agilent). Libraries were prepared using the TruSeq RNA Sample Preparation v2 kit (Illumina). The library quality was checked using High Sensitivity DNA chips on a Bioanalyzer. The sample concentration was measured with a Qubit dsDNA HS Assay Kit and adjusted to 2 nM before sequencing (50 bp) on a HiSeq 2000 (Illumina) according to the manufacturer's instructions.

Differential gene expression analysis

The differential gene expression analysis was performed as previously described (57). Briefly, RNA-seq data were aligned to the genome using STAR with default options, generating mapping files (BAM format). Differential expression Read counts were generated using FeaturesCount (http://bioinf.wehi.edu.au/featureCounts/) and samples were compared for differential expression using DESeq2 (58). Genes with a P-value ≤ 0.05 and a mean read count ≥ 10 were considered to be differentially expressed.

Networks analysis

Additional network analysis was performed for the 500 most significant genes using the bioinformatics tool ToppGene Suite (59). For this analysis, we considered upregulated and downregulated genes separately. Functional enrichment analysis was then conducted on those genes through DAVID (60).

Real-time PCR

To assess gene expression via qPCR, RNA was reverse transcribed with a QuantiTect Reverse Transcription kit (Qiagen), following the protocol provided by the manufacture. cDNA was then added to a qPCR reaction mixture, according to the Mesa Blue qPCR MasterMix Plus for SYBR Assay (Eurogentec) instructions. Custom primers for genes of interest were designed and checked for target specificity using the bioinformatics tool Primer-Blast (61). The following sequences of primers were used: FOXM1 5′-GCACTTGGAATCACAGCAGA-3′/5′-CACCGGGAACTGGATAGGTA-3′; BRCA2 5′-AGCAGATGATGTTTCCTGTCC-3′/5′-TCTGACGACCCTTCACAAAC-3′; TOP2A 5′-GCCCATTGGTCAGTTTGGTA-3′/5′-AATCGAGCCAAAGAGCTGAG-3′; and B-actin 5′-GCGAGAAGATGACCCAGATC-3′/5′-CCAGTGGTACGGCCAGAGG-3′. qPCRs were carried out in a Mx300P cycler (Agilent Techonolgy), equipped with a MxPro software, with the following settings: 5 min at 95°C, 40 cycles of 30 s at 95°C and 1.5 min at 60°C. cDNA from at least three independent experiments was tested and each sample was ran in triplicates. The Livak method ($2^{-\Delta\Delta Ct}$) was used to perform relative quantification of genes (62).

Single cell gel electrophoresis

DNA single- and double-strand breaks were detected via single cell gel electrophoresis (comet) assay, according to the guidelines provided in (54). Adherent slides were coated with 1% low-gelling temperature agarose (PeqLab) and allowed to dry. LUHMES cells harvested in PBS were mixed with 1% agarose and placed on a precoated slide. After agarose gelling, slides were submerged in alkaline lysis buffer (1.2 M NaCl, 100 mM Na_2EDTA, 0.1% sodium lauryl sarcosinate, 0.26 M NaOH,

pH > 13) and placed overnight at 4°C. Slices were then washed 3 times with rinse solution (0.03 M NaOH, 2 mM Na_2EDTA, pH = 12.3). Electrophoresis was carried out for 25 min at a constant voltage of 0.6 V/cm. Slides were removed from the electrophoresis chamber, neutralized with distilled water and stained with 2.5 μg/mL of propidium iodide, for 20 min at RT. Excess of stain was removed by rinsing the slides with distilled water. For each slide, at least 50 comet images were acquired in an epifluorescence microscope (Leica DMI 6000B microscope, Leica). Tail moment (the product of the percentage of DNA in the tail and the tail length) of each individual comet was determined using the CometScore software (TriTek Corp).

Reactive oxygen species detection

Differentiated LUHMES cells seeded in 96-well plates were washed once with warm PBS. For measuring total ROS production, cells were incubated with 25 μM DCFDA (Sigma), for 25 min at 37°C, whereas miROS was measured by incubating cells with 1 μM MitoSOX Red probe (Invitrogen), for 20 min at 37°C. After incubation time, excess of probe was removed by washing the cells with PBS. Fluorescence measurements were performed using an Infinite M2000 PRO (Tecan Ltd). To detect total ROS, the excitation and emission wavelengths were set to 485 and 535 nm, respectively. miROS was measured by using 510 nm for excitation and 580 nm for emission wavelength. Following three basal measurements, cells were challenged with 5% H_2O_2 and fluorescence values were recorded up to 30 min, at indicated time points.

Statistical analysis

Data are presented as mean ± standard deviation (SD) of, at least, three independent experiments. One- or two-way ANOVA test, with Bonferroni correction, were applied to determine significance of differences using GraphPad Prism 5 software. Unless otherwise, stated P-value < 0.05 was considered to indicate a significant difference.

Supplementary Material

Supplementary Material is available at *HMG* online.

Acknowledgements

We thank Anne-Christine Flach and Sindhu Thiagarajan for technical assistance with cell sorting and cell culture.

Conflict of Interest statement. None declared.

Funding

R.P. was supported by a PhD fellowship from Fundação para a Ciência e a Tecnologia (SFRH/BD/80884/2011). T.F.O. is supported by the Deutsche Forschungsgemeinschaft - Center for Nanoscale Microscopy and Molecular Physiology of the Brain (CNMPB) and by Federal Ministry of Education and Research (BMBF) Grant Decipher PD (01KU1503B).

References

1. Smith, Y., Wichmann, T., Factor, S.A. and DeLong, M.R. (2012) Parkinson's disease therapeutics: new developments and challenges since the introduction of levodopa. *Neuropsychopharmacology*, **37**, 213–246.
2. Chaudhuri, K.R., Healy, D.G., Schapira, A.H. and National Institute for Clinical, E. (2006) Non-motor symptoms of Parkinson's disease: diagnosis and management. *Lancet Neurol.*, **5**, 235–245.
3. Villar-Pique, A., Lopes da Fonseca, T. and Outeiro, T.F. (2016) Structure, function and toxicity of alpha-synuclein: the Bermuda triangle in synucleinopathies. *J. Neurochem.*, **139** (Suppl 1), 240–255.
4. Yacoubian, T.A., Cantuti-Castelvetri, I., Bouzou, B., Asteris, G., McLean, P.J., Hyman, B.T. and Standaert, D.G. (2008) Transcriptional dysregulation in a transgenic model of Parkinson disease. *Neurobiol. Dis.*, **29**, 515–528.
5. Miller, R.M., Kiser, G.L., Kaysser-Kranich, T., Casaceli, C., Colla, E., Lee, M.K., Palaniappan, C. and Federoff, H.J. (2007) Wild-type and mutant alpha-synuclein induce a multi-component gene expression profile consistent with shared pathophysiology in different transgenic mouse models of PD. *Exp. Neurol.*, **204**, 421–432.
6. Grunblatt, E., Mandel, S., Jacob-Hirsch, J., Zeligson, S., Amariglo, N., Rechavi, G., Li, J., Ravid, R., Roggendorf, W., Riederer, P. *et al.* (2004) Gene expression profiling of parkinsonian substantia nigra pars compacta; alterations in ubiquitin-proteasome, heat shock protein, iron and oxidative stress regulated proteins, cell adhesion/cellular matrix and vesicle trafficking genes. *J. Neural Transm.*, **111**, 1543–1573.
7. Pinho, R., Guedes, L.C., Soreq, L., Lobo, P.P., Mestre, T., Coelho, M., Rosa, M.M., Goncalves, N., Wales, P., Mendes, T. *et al.* (2016) Gene expression differences in peripheral blood of Parkinson's disease patients with distinct progression profiles. *PLoS One*, **11**, e0157852.
8. Soreq, L., Ben-Shaul, Y., Israel, Z., Bergman, H. and Soreq, H. (2012) Meta-analysis of genetic and environmental Parkinson's disease models reveals a common role of mitochondrial protection pathways. *Neurobiol. Dis.*, **45**, 1018–1030.
9. Jin, H., Kanthasamy, A., Ghosh, A., Yang, Y., Anantharam, V. and Kanthasamy, A.G. (2011) alpha-Synuclein negatively regulates protein kinase Cdelta expression to suppress apoptosis in dopaminergic neurons by reducing p300 histone acetyltransferase activity. *J. Neurosci.*, **31**, 2035–2051.
10. Hashimoto, M., Hsu, L.J., Rockenstein, E., Takenouchi, T., Mallory, M. and Masliah, E. (2002) alpha-Synuclein protects against oxidative stress via inactivation of the c-Jun N-terminal kinase stress-signaling pathway in neuronal cells. *J. Biol. Chem.*, **277**, 11465–11472.
11. Kim, S.S., Moon, K.R. and Choi, H.J. (2011) Interference of alpha-synuclein with cAMP/PKA-dependent CREB signaling for tyrosine hydroxylase gene expression in SK-N-BE(2)C cells. *Arch. Pharm. Res.*, **34**, 837–845.
12. Decressac, M., Kadkhodaei, B., Mattsson, B., Laguna, A., Perlmann, T. and Bjorklund, A. (2012) alpha-Synuclein-induced down-regulation of Nurr1 disrupts GDNF signaling in nigral dopamine neurons. *Sci. Transl. Med.*, **4**, 163ra156.
13. Eschbach, J., von Einem, B., Muller, K., Bayer, H., Scheffold, A., Morrison, B.E., Rudolph, K.L., Thal, D.R., Witting, A., Weydt, P. *et al.* (2015) Mutual exacerbation of peroxisome proliferator-activated receptor gamma coactivator 1alpha deregulation and alpha-synuclein oligomerization. *Ann. Neurol.*, **77**, 15–32.
14. Siddiqui, A., Chinta, S.J., Mallajosyula, J.K., Rajagopolan, S., Hanson, I., Rane, A., Melov, S. and Andersen, J.K. (2012)

Selective binding of nuclear alpha-synuclein to the PGC1alpha promoter under conditions of oxidative stress may contribute to losses in mitochondrial function: implications for Parkinson's disease. *Free Radic. Biol. Med.*, **53**, 993–1003.
15. Baptista, M.J., O'Farrell, C., Daya, S., Ahmad, R., Miller, D.W., Hardy, J., Farrer, M.J. and Cookson, M.R. (2003) Co-ordinate transcriptional regulation of dopamine synthesis genes by alpha-synuclein in human neuroblastoma cell lines. *J. Neurochem.*, **85**, 957–968.
16. Pavlou, M.A., Pinho, R., Paiva, I. and Outeiro, T.F. (2017) The yin and yang of alpha-synuclein-associated epigenetics in Parkinson's disease. *Brain*, **140**, 878–886.
17. Goers, J., Manning-Bog, A.B., McCormack, A.L., Millett, I.S., Doniach, S., Di Monte, D.A., Uversky, V.N. and Fink, A.L. (2003) Nuclear localization of alpha-synuclein and its interaction with histones. *Biochemistry*, **42**, 8465–8471.
18. Liu, X., Lee, Y.J., Liou, L.C., Ren, Q., Zhang, Z., Wang, S. and Witt, S.N. (2011) Alpha-synuclein functions in the nucleus to protect against hydroxyurea-induced replication stress in yeast. *Hum. Mol. Genet.*, **20**, 3401–3414.
19. Kontopoulos, E., Parvin, J.D. and Feany, M.B. (2006) Alpha-synuclein acts in the nucleus to inhibit histone acetylation and promote neurotoxicity. *Hum. Mol. Genet.*, **15**, 3012–3023.
20. Falkenberg, K.J. and Johnstone, R.W. (2014) Histone deacetylases and their inhibitors in cancer, neurological diseases and immune disorders. *Nat. Rev. Drug Discov.*, **13**, 673–691.
21. Robert, C. and Rassool, F.V. (2012) HDAC inhibitors: roles of DNA damage and repair. *Adv. Cancer Res.*, **116**, 87–129.
22. Monti, B., Gatta, V., Piretti, F., Raffaelli, S.S., Virgili, M. and Contestabile, A. (2010) Valproic acid is neuroprotective in the rotenone rat model of Parkinson's disease: involvement of alpha-synuclein. *Neurotox. Res.*, **17**, 130–141.
23. Chen, P.S., Wang, C.C., Bortner, C.D., Peng, G.S., Wu, X., Pang, H., Lu, R.B., Gean, P.W., Chuang, D.M. and Hong, J.S. (2007) Valproic acid and other histone deacetylase inhibitors induce microglial apoptosis and attenuate lipopolysaccharide-induced dopaminergic neurotoxicity. *Neuroscience*, **149**, 203–212.
24. Scholz, D., Poltl, D., Genewsky, A., Weng, M., Waldmann, T., Schildknecht, S. and Leist, M. (2011) Rapid, complete and large-scale generation of post-mitotic neurons from the human LUHMES cell line. *J. Neurochem.*, **119**, 957–971.
25. Masliah, E., Rockenstein, E., Veinbergs, I., Mallory, M., Hashimoto, M., Takeda, A., Sagara, Y., Sisk, A. and Mucke, L. (2000) Dopaminergic loss and inclusion body formation in alpha-synuclein mice: implications for neurodegenerative disorders. *Science*, **287**, 1265–1269.
26. Zhang, Z., Li, X., Xie, W.J., Tuo, H., Hintermann, S., Jankovic, J. and Le, W. (2012) Anti-parkinsonian effects of Nurr1 activator in ubiquitin-proteasome system impairment induced animal model of Parkinson's disease. *CNS Neurol. Disord. Drug Targets*, **11**, 768–773.
27. Hashimoto, M., Takenouchi, T., Rockenstein, E. and Masliah, E. (2003) Alpha-synuclein up-regulates expression of caveolin-1 and down-regulates extracellular signal-regulated kinase activity in B103 neuroblastoma cells: role in the pathogenesis of Parkinson's disease. *J. Neurochem.*, **85**, 1468–1479.
28. Ding, H., Fineberg, N.S., Gray, M. and Yacoubian, T.A. (2013) alpha-Synuclein overexpression represses 14-3-3theta transcription. *J. Mol. Neurosci.*, **51**, 1000–1009.
29. Ma, Y., Dhawan, V., Mentis, M., Chaly, T., Spetsieris, P.G. and Eidelberg, D. (2002) Parametric mapping of [18F]FPCIT binding in early stage Parkinson's disease: a PET study. *Synapse*, **45**, 125–133.
30. Hegde, M.L., Hegde, P.M., Rao, K.S. and Mitra, S. (2011) Oxidative genome damage and its repair in neurodegenerative diseases: function of transition metals as a double-edged sword. *J. Alzheimers Dis.*, **24(Suppl. 2)**, 183–198.
31. Pettifer, K.M., Jiang, S., Bau, C., Ballerini, P., D'Alimonte, I., Werstiuk, E.S. and Rathbone, M.P. (2007) MPP(+)-induced cytotoxicity in neuroblastoma cells: antagonism and reversal by guanosine. *Purinergic Signal.*, **3**, 399–409.
32. Sugars, K.L. and Rubinsztein, D.C. (2003) Transcriptional abnormalities in Huntington disease. *Trends Genet.*, **19**, 233–238.
33. Chen, X.F., Zhang, Y.W., Xu, H. and Bu, G. (2013) Transcriptional regulation and its misregulation in Alzheimer's disease. *Mol. Brain*, **6**, 44.
34. Desplats, P., Spencer, B., Crews, L., Pathel, P., Morvinski-Friedmann, D., Kosberg, K., Roberts, S., Patrick, C., Winner, B., Winkler, J. *et al.* (2012) alpha-Synuclein induces alterations in adult neurogenesis in Parkinson disease models via p53-mediated repression of Notch1. *J. Biol. Chem.*, **287**, 31691–31702.
35. Lee, S.S., Kim, Y.M., Junn, E., Lee, G., Park, K.H., Tanaka, M., Ronchetti, R.D., Quezado, M.M. and Mouradian, M.M. (2003) Cell cycle aberrations by alpha-synuclein over-expression and cyclin B immunoreactivity in Lewy bodies. *Neurobiol. Aging*, **24**, 687–696.
36. Madabhushi, R., Pan, L. and Tsai, L.H. (2014) DNA damage and its links to neurodegeneration. *Neuron*, **83**, 266–282.
37. Weissman, L., de Souza-Pinto, N.C., Stevnsner, T. and Bohr, V.A. (2007) DNA repair, mitochondria, and neurodegeneration. *Neuroscience*, **145**, 1318–1329.
38. Nakanishi, A., Minami, A., Kitagishi, Y., Ogura, Y. and Matsuda, S. (2015) BRCA1 and p53 tumor suppressor molecules in Alzheimer's disease. *Int. J. Mol. Sci.*, **16**, 2879–2892.
39. Feng, D.D., Cai, W. and Chen, X. (2015) The associations between Parkinson's disease and cancer: the plot thickens. *Transl. Neurodegener.*, **4**, 20.
40. Sepe, S., Milanese, C., Gabriels, S., Derks, K.W., Payan-Gomez, C., van, I.W.F., Rijksen, Y.M., Nigg, A.L., Moreno, S., Cerri, S. *et al.* (2016) Inefficient DNA repair is an aging-related modifier of Parkinson's disease. *Cell Rep.*, **15**, 1866–1875.
41. Martin, F.L., Williamson, S.J., Paleologou, K.E., Hewitt, R., El-Agnaf, O.M. and Allsop, D. (2003) Fe(II)-induced DNA damage in alpha-synuclein-transfected human dopaminergic BE(2)-M17 neuroblastoma cells: detection by the Comet assay. *J. Neurochem.*, **87**, 620–630.
42. Moller, P., Loft, S., Ersson, C., Koppen, G., Dusinska, M. and Collins, A. (2014) On the search for an intelligible comet assay descriptor. *Front. Genet.*, **5**, 217.
43. Protter, D., Lang, C. and Cooper, A.A. (2012) alphaSynuclein and mitochondrial dysfunction: a pathogenic partnership in *Parkinson's disease? Parkinsons Dis.*, **2012**, 829207.
44. Moon, H.E. and Paek, S.H. (2015) Mitochondrial dysfunction in Parkinson's disease. *Exp. Neurobiol.*, **24**, 103–116.
45. Devi, L., Raghavendran, V., Prabhu, B.M., Avadhani, N.G. and Anandatheerthavarada, H.K. (2008) Mitochondrial import and accumulation of alpha-synuclein impair complex I in human dopaminergic neuronal cultures and Parkinson disease brain. *J. Biol. Chem.*, **283**, 9089–9100.
46. Chinta, S.J., Mallajosyula, J.K., Rane, A. and Andersen, J.K. (2010) Mitochondrial alpha-synuclein accumulation impairs complex I function in dopaminergic neurons and results in increased mitophagy in vivo. *Neurosci. Lett.*, **486**, 235–239.

47. Martin, L.J., Pan, Y., Price, A.C., Sterling, W., Copeland, N.G., Jenkins, N.A., Price, D.L. and Lee, M.K. (2006) Parkinson's disease alpha-synuclein transgenic mice develop neuronal mitochondrial degeneration and cell death. *J. Neurosci.*, **26**, 41–50.
48. Yasuda, T. and Mochizuki, H. (2010) The regulatory role of alpha-synuclein and parkin in neuronal cell apoptosis; possible implications for the pathogenesis of Parkinson's disease. *Apoptosis*, **15**, 1312–1321.
49. Bernstein, C., Bernstein, H., Payne, C.M. and Garewal, H. (2002) DNA repair/pro-apoptotic dual-role proteins in five major DNA repair pathways: fail-safe protection against carcinogenesis. *Mutat. Res.*, **511**, 145–178.
50. Parihar, M.S., Parihar, A., Fujita, M., Hashimoto, M. and Ghafourifar, P. (2008) Mitochondrial association of alpha-synuclein causes oxidative stress. *Cell Mol. Life Sci.*, **65**, 1272–1284.
51. Pfefferkorn, C.M., Jiang, Z. and Lee, J.C. (2012) Biophysics of alpha-synuclein membrane interactions. *Biochim. Biophys. Acta*, **1818**, 162–171.
52. Outeiro, T.F. and Lindquist, S. (2003) Yeast cells provide insight into alpha-synuclein biology and pathobiology. *Science*, **302**, 1772–1775.
53. Wang, C. and Youle, R.J. (2009) The role of mitochondria in apoptosis*. *Annu. Rev. Genet.*, **43**, 95–118.
54. Oliveira, J.M., Chen, S., Almeida, S., Riley, R., Goncalves, J., Oliveira, C.R., Hayden, M.R., Nicholls, D.G., Ellerby, L.M. and Rego, A.C. (2006) Mitochondrial-dependent Ca2+ handling in Huntington's disease striatal cells: effect of histone deacetylase inhibitors. *J. Neurosci.*, **26**, 11174–11186.
55. Zufferey, R., Dull, T., Mandel, R.J., Bukovsky, A., Quiroz, D., Naldini, L. and Trono, D. (1998) Self-inactivating lentivirus vector for safe and efficient in vivo gene delivery. *J. Virol.*, **72**, 9873–9880.
56. Lizee, G., Aerts, J.L., Gonzales, M.I., Chinnasamy, N., Morgan, R.A. and Topalian, S.L. (2003) Real-time quantitative reverse transcriptase-polymerase chain reaction as a method for determining lentiviral vector titers and measuring transgene expression. *Hum. Gene Ther.*, **14**, 497–507.
57. Halder, R., Hennion, M., Vidal, R.O., Shomroni, O., Rahman, R.U., Rajput, A., Centeno, T.P., van Bebber, F., Capece, V., Garcia Vizcaino, J.C. *et al.* (2016) DNA methylation changes in plasticity genes accompany the formation and maintenance of memory. *Nat. Neurosci.*, **19**, 102–110.
58. Love, M.I., Huber, W. and Anders, S. (2014) Moderated estimation of fold change and dispersion for RNA-seq data with DESeq2. *Genome Biol.*, **15**, 550.
59. Chen, J., Bardes, E.E., Aronow, B.J. and Jegga, A.G. (2009) ToppGene Suite for gene list enrichment analysis and candidate gene prioritization. *Nucleic Acids Res.*, **37**, W305–W311.
60. Huang da, W., Sherman, B.T. and Lempicki, R.A. (2009) Systematic and integrative analysis of large gene lists using DAVID bioinformatics resources. *Nat. Protoc.*, **4**, 44–57.
61. Ye, J., Coulouris, G., Zaretskaya, I., Cutcutache, I., Rozen, S. and Madden, T.L. (2012) Primer-BLAST: a tool to design target-specific primers for polymerase chain reaction. *BMC Bioinformatics*, **13**, 134.
62. Livak, K.J. and Schmittgen, T.D. (2001) Analysis of relative gene expression data using real-time quantitative PCR and the 2(-Delta Delta C(T)) method. *Methods*, **25**, 402–408.